



# RXR $\gamma$ attenuates cerebral ischemia–reperfusion induced ferroptosis in neurons in mice through transcriptionally promoting the expression of GPX4

Lei Yang<sup>1,2</sup> · Baoshun Du<sup>3</sup> · Shitao Zhang<sup>4</sup> · Maode Wang<sup>1</sup>

Received: 12 January 2022 / Accepted: 17 April 2022 / Published online: 29 April 2022

© The Author(s), under exclusive licence to Springer Science+Business Media, LLC, part of Springer Nature 2022

## Abstract

Cerebral ischemia is a common cerebrovascular disease with high mortality and disability rate. Exploring its mechanism is essential for developing effective treatment for cerebral ischemia. Therefore, this study aims to explore the regulatory effect and mechanism of retinoid X receptor  $\gamma$  (RXR $\gamma$ ) on cerebral ischemia–reperfusion (I/R) injury. A mouse intraluminal middle cerebral artery occlusion model was established, and PC12 cells were exposed to anaerobic/reoxygenation (A/R) as an in vitro model in this study. Cerebral I/R surgery or A/R treatment induced ferroptosis, downregulated RXR $\gamma$  and GPX4 (glutathione peroxidase 4) levels, upregulated cyclooxygenase-2 (COX-2) level and increased ROS (reactive oxygen species) level in A/R induced cells or I/R brain tissues in vivo or PC12 cells in vitro. Knockdown of RXR $\gamma$  downregulated GPX4 and increased COX-2 and ROS levels in A/R induced cells. RXR $\gamma$  overexpression has the opposite effect. GPX4 knockdown reversed the improvement of RXR $\gamma$  overexpression on COX-2 downregulation, GPX4 upregulation and ferroptosis in PC12 cells. Furthermore, chromatin immunoprecipitation (ChIP) and luciferase reporter gene assays revealed that RXR $\gamma$  bound to GPX4 promoter region and activated its transcription. Overexpression of RXR $\gamma$  or GPX4 alleviated brain damage and inhibited ferroptosis in I/R mice. In conclusion, RXR $\gamma$ -mediated transcriptional activation of GPX4 might inhibit ferroptosis during I/R-induced brain injury.

**Keywords** RXR $\gamma$  · Ischemia–reperfusion · Ferroptosis · GPX4 · Mice

## Introduction

Cerebral ischemia has the characteristics of high mortality and high disability rate, which seriously endangers human health. The severity of brain injury depends on

the degree of primary ischemic injury and the intensity of delayed cell damage caused by secondary reperfusion injury. Hypoxic ischemic stroke is a frequently-occurring disease in the elderly. Ischemia–reperfusion (I/R) injury is the main mechanism of most cerebrovascular diseases. However, I/R induces a variety of cellular responses in the brain (Kalogeris et al. 2016). The mechanisms involved in the injury are disorder of energy metabolism, inflammatory response, free radical injury, toxic effect of excitatory amino acids, iron deposition, etc. (Bi et al. 2019). During the recovery of blood and oxygen, a large number of oxygen free radicals produced by enzymatic reaction cause the peroxidation of polyunsaturated fatty acids or plasma lipoproteins, and then lead to the damage of cell membrane, intracellular protein and even DNA (Duan et al. 2019).

Recent researches showed that iron overload was a main source of oxidative stress in ischemic brain and played an important role in the brain injury mediated by I/R (Wang et al. 2021b; Li et al. 2020). When the brain neuron is anoxic, the consumption of oxygen and nutrients leads to mitochondrial injury, oxidative stress

✉ Maode Wang  
maode\_wang@126.com

<sup>1</sup> Department of Neurosurgery, The First Affiliated Hospital of Xi'an Jiaotong University, No. 277 Yanta West Road, Yanta District, Xi'an City, Shaanxi Province 710061, People's Republic of China

<sup>2</sup> Department of Neurosurgery, The Second Affiliated Hospital of Xi'an Medical University, Xi'an City, Shaanxi Province 710038, People's Republic of China

<sup>3</sup> Second Department of Neurosurgery, Xinxiang Central Hospital, Xinxiang, Henan Province 453003, People's Republic of China

<sup>4</sup> Department of Neurosurgery, Xi'an No.3 hospital, the Affiliated Hospital of Northwest University, Xi'an City, Shaanxi Province 710018, People's Republic of China

or neuron loss, and necrosis, apoptosis, autophagy and ferroptosis may occur in the cells.

Studies have found that iron level in the brain of animal models of cerebral ischemia and patients is increased (Dai et al. 2019; Lu et al. 2020), and changes in iron and iron metabolism-related proteins during cerebral ischemia lead to increased iron content in brain tissue and iron deposition in neurons, causing neuronal damage and excessive production (Dai et al. 2019). The products of the free radicals invade lipids, DNA and proteins, causing severe oxidative damage and oxidative stress, and even death. Ferroptosis is a new type of programmed cell death, which is iron dependent and different from apoptosis, necrosis and autophagic death. It is based on increased intracellular ferrous ion ( $\text{Fe}^{2+}$ ) concentration (iron deposition), reactive oxygen species (ROS) accumulation, and lipid peroxidation. The main mechanism of ferroptosis is that under the action of divalent iron or ester oxygenase, the unsaturated fatty acids highly expressed on the cell membrane were catalyzed to produce lipid peroxidation and induce cell death. In terms of cell morphology, ferroptosis leads to significant reduction in mitochondria size, the increase in mitochondrial membrane density and the decrease in cristae. Ferroptosis is now considered to be a key link in cerebral ischemia-hypoxic injury and an important factor affecting the recovery of ischemic-hypoxic stroke.

Retinol X receptor (RXR) is a ligand-induced transcription factor, which is a member of the nuclear receptor superfamily. RXR is mainly composed of  $\text{RXR}\alpha$ ,  $\text{RXR}\beta$  and  $\text{RXR}\gamma$ . The RXR subtype can respond to the same ligand, so it can regulate transcription of the same target gene. However, the expression patterns of these three subtypes in various tissues are quite different.  $\text{RXR}\alpha$  is predominantly expressed in visceral tissues such as epidermis, intestine, kidney and liver;  $\text{RXR}\beta$  expression is widely distributed;  $\text{RXR}\gamma$  is mainly expressed in brain and skeletal muscle. A study has shown that nuclear  $\text{RXR}\alpha$  and  $\text{RXR}\beta$  have different and opposite effects on RA-mediated neuroblastoma differentiation (Girardi et al. 2019). As a transcription factor, RXR can be activated by specific ligands, and then combined with specific DNA sequences to transactivate the transcription of its target genes. RXR ligands (agonists or antagonists) exert various physiological functions according to their partner receptors, making RXR participate in the transcription regulation of many processes in the body and play a central role in the pathogenesis of metabolic disorders, cardiovascular diseases, diabetes, and inflammation in the body. However, the research of  $\text{RXR}\gamma$  in ischemia/reperfusion injury is not extensive.

Genetic studies in cells and mice have shown that the selenase glutathione peroxidase (GPX4) is a key regulator of ferroptosis (Maiorino et al. 2018). Lipid hydroperoxidase

GPX4 converts lipid hydroperoxides into lipid alcohols, which can prevent the formation of iron ( $\text{Fe}^{2+}$ ) dependent toxic lipid reactive oxygen species (ROS) (Ding et al. 2020). Inhibition of GPX4 function can lead to lipid peroxidation, and may lead to the induction of ferroptosis, iron dependent non apoptotic form of cell death (Forcina and Dixon 2019). GPX4 deletion induced lipid peroxidation dependent cell death in mouse embryo, testis, brain, liver, heart and photoreceptor cells. Bioinformatics analysis revealed that  $\text{RXR}\gamma$  may be associated with GPX4 expression. In this study, we tried to explore the role of  $\text{RXR}\gamma$  in regulating GPX4-mediated ferroptosis during cerebral I/R injury. We confirmed that  $\text{RXR}\gamma$ -induced transcriptional activation of GPX4 alleviated cerebral I/R injury by reducing ferroptosis. Our research provides a new idea for the mechanism of brain I/R and the development of treatment for ischemic stroke in the future.

## Materials and methods

### Intraluminal middle cerebral artery occlusion model

Adult 6- to 8-week-old male C57BL/6 J mice, weighing 20–25 g, were housed under diurnal lighting conditions with 12 h of light (lights on at 7:00 AM) and allowed access to food and water ad libitum. The middle cerebral artery occlusion (MCAO) model used was previously developed and described (Rousselet et al. 2012). Briefly, after mice were deeply anesthetized with 10% chloral hydrate (100 mL/kg, intraperitoneal injection), their fur and skin were disinfected with povidone-iodine (Betadine, Purdue Frederick Company, Norwalk, CT, USA). A mid-line neck incision was made, and the soft tissues were retracted. The common carotid artery, bifurcation of the internal common carotid artery (ICA), and external common carotid artery (ECA) were carefully dissected. The ECA was temporarily occluded using a 5–0 silk suture. The ICA was clipped using reverse-action tweezers to minimize bleeding. A small hole was cut into the ECA for the insertion of a silicone-coated filament (Beijing Cinontech Co.Ltd, Beijing, China) into the ICA. The suture was tightly tied around the monofilament to prevent bleeding, and the reverse-action tweezers were removed. After 90 min, the suture was removed for reperfusion, and the wound and skin were closed. The body temperature of the mice was maintained between 37.0 °C and 37.5 °C with a heating pad during surgery. For sham operations, all procedures were identical except that the occluding monofilament was not inserted. All procedures in this study were conducted in accordance with the First Affiliated Hospital of Xi'an Jiaotong University (Xi'an, China) of ethics committee's approved protocols (XJTULAC-2020–053).

## Grouping and model establishment of AR model

PC12 cells, provided by the institution called American Type Culture Collection (ATCC), were cultured in Dulbecco's modified Eagle's medium supplemented with 10% fetal bovine serum (FBS) in an incubator with 5% CO<sub>2</sub> and saturated humidity at 37 °C, and the medium was replenished once every 3 days. The cells were maintained in DMEM supplemented with 10% (v/v) FBS, 100 U/ml penicillin and 100 µg/mL streptomycin in a humidified incubator under 5% CO<sub>2</sub> at 37 °C. Then, AR-induced PC12 cells were constructed 48 h after A/R treatment, incubated for 2 h in a tri-gas incubator containing 1% O<sub>2</sub>, 94% N<sub>2</sub>, and 5% CO<sub>2</sub> (Thermo Fisher Scientific, San Jose, CA), and placed in the incubator with 5% CO<sub>2</sub>, 21% O<sub>2</sub>, and 74% N<sub>2</sub> for another 6, 12 or 24 h. PC12 cells were assigned into six groups: (a) Control group: Cells cultured in normal medium without any treatment; (b) A/R 6 h group: Cells induced by A/R for 6 h; (c) A/R 12 h group: Cells induced by A/R for 12 h; (d) A/R 24 h group: Cells induced by A/R for 24 h. 0.2 or 0.5 µg/mL RXR $\gamma$  shRNA and NC shRNA (a negative control of RXR $\gamma$  shRNA), pcDNA-RXR $\gamma$  (RXR $\gamma$ ) and pcDNA3.1 (Vector) were constructed by Cyagen Biosciences Inc. (Guangzhou, China).

## RNA extraction and Quantitative real-time polymerase chain reaction (RT-qPCR)

Total RNA was extracted from cells or tissues in strict accordance with the instructions of Trizol reagent (Invitrogen, Carlsbad, CA, USA) and purified with RNeasy Maxi Kit (Qiagen, Dusseldorf, Germany) according to the manufacturer's agreement. 1 µg of total RNA of each sample was reversely-transcribed using M-MLV Reverse Transcriptase (Invitrogen, Carlsbad, CA, USA), and FGD5-AS1 expression was detected by using Bio-Rad (Hercules, CA) IQ SYBR Green Supermix with Opticon (MJ Research, Waltham, MA, USA) according to the manufacturer's protocols. GAPDH was used as an endogenous control. In real-time PCR system (ABI7500, Applied Biosystems, Waltham, MA, USA), the detailed process was as follows: 1 min at 95 °C, 20 s at 95 °C, 35 cycles, then 10 s at 56 °C and 15 s at 72 °C. Finally, the relative expression of GPX4 was calculated using the  $2^{-\Delta\Delta C_t}$  method. GPX4 F: 5'-GTG GAA CTT CAC CAA GTT TGG AC-3'; GPX4 R: 5'-GGG CAG GTC CTT CTC TAT CAC-3'; GAPDH F: 5'-AGC CCA AGA TGC CCT TCA GT-3', GAPDH R: 5'-CCG TGT TCC TAC CCC CAA TG-3'.

## Western blotting

First of all, RIPA lysis buffer (CW biotechnology, Beijing, China) was used to extract the total protein from the cells, and then the protein concentration was determined by BCA

protein analysis kit (Thermo Fisher Scientific, Waltham, Massachusetts, USA). 10% SDS-PAGE was used to separate the protein samples at 120 V for 160 min. Next, we transfer the complex onto the nitrocellulose membrane (General Electric Co, USA). After being sealed with 5% skim milk, the imprint was detected with primary antibody. The primary antibodies used in this study including Rabbit monoclonal to RXR $\gamma$  (1:300, Antibody #5629, Cell Signaling Technology (CST), Boston, MA, USA), Rabbit monoclonal to COX2 (1:400, ab188183, Abcam, Cambridge, UK), GPX4 (1:300, ab252833, Abcam), Rabbit monoclonal to  $\beta$ -tubulin (1:300, ab179513, Abcam). Then, HRP-conjugated goat anti-rabbit IgG (ab205718, 1:1000, Abcam) was incubated for 2 h at room temperature. The protein bands were visualized with enhanced chemiluminescence reagents (Pierce, Rockford, IL, USA) and analyzed with ImageJ software (National Institutes of Health, Bethesda, MD, USA).  $\beta$ -tubulin was used as an endogenous control to normalize protein expression.

## ROS detection

Dichloro-dihydro-fluorescein diacetate (DCFH-DA; Beijing Beyotime Biotechnology, Beijing, China) was used to determine the intracellular ROS levels. At first, PC12 cells were seeded into 24-well plates, washed with serum-free DMEM culture medium, diluted to 1 µmol/L with serum-free DMEM, and incubated for 30 min at 37 °C in avoidance of light. Next, five visual fields were selected for observation under a fluorescence microscope and photos taken were analyzed by using the software ImageJ 1.41 (NIH, Bethesda, MD) to obtain the mean fluorescence density of each visual field.

## Immunofluorescence assay

The immunostaining procedure was performed as previously described (Burton et al. 2011). At the indicated times after MCAO, the brains were removed quickly and post-fixed in 4% paraformaldehyde overnight. The brains were then dehydrated in a gradient sucrose solution (10%, 20%, and 30%) at 4 °C. Serial sections of the mouse brain (10 µm thick) were cut using a cryostat. Microscope slides with mounted brain slices were stored temporarily in cryoprotectant solution at 30 °C until use for morphological staining. After rinsing with 0.3% Triton X-100 for 30 min at 37 °C, the sections were blocked in a solution containing 5% normal goat serum for 1 h, and then washed several times. The sections were incubated with the following primary antibodies at 4 °C overnight: rabbit polyclonal anti-DAPI (1:400, #4850, Cell Signaling Technology (CST), Boston, MA, USA), rabbit monoclonal anti-GAPDH (ab181602, 1:400, Abcam, Cambridge, UK), and rabbit monoclonal anti-MAP2 (microtubule association protein-2) (ab183830, 1:300, Abcam). The primary antibodies were detected by Alexa488- and

Alexa594-conjugated secondary antibodies (1:1000) at room temperature for 1 h. The sections were coverslipped with glycerol, and the immunofluorescence was detected using an Olympus BX5 microscope. The percentage of apoptotic neurons was determined for each group of each repeated experiment (200× magnification).

For immunocytochemistry, the cells were washed twice with PBS, fixed with 4% paraformaldehyde for 20 min, and then blocked with 5% goat serum albumin for 1 h. The cells were then incubated with antibodies at 4 °C overnight, washed 3 times with PBS, incubated with rat anti-rabbit Cy3-conjugated secondary antibodies (1:1,000) for 1 h in a 37 °C thermostat-controlled incubator, and finally coverslipped with an anti-fluorescence-quenching reagent (Boshide, China). After staining the cell nuclei with 4',6-diamidino-2-phenylindole (DAPI), the fluorescent images were detected and analyzed as described above. For each repeated experiment, the cells were counted in 5 random fields (200× magnification).

For terminal deoxynucleotidyl transferase dUTP nick end labeling (TUNEL) assays, samples obtained following A/R or MCAO were double stained using a NeuN and TUNEL kit, according to the manufacturer's instructions. The fluorescence imaging procedure was performed and analyzed as described above.

### Enzyme-linked immunosorbent assay (ELISA)

ELISA kits were used to detect the contents of VEGFA, IL-1 $\beta$  and IL-6 in cells, tissues and serum. All the reagents were purchased from the company of Thermo Fisher Scientific (Waltham, MA, USA), and the operation method was carried out according to the manual.

### Cell proliferation and invasion

CCK-8 cell proliferation assay kit was used to detect cell proliferation. After the cells were cultured for 24 h,  $3 \times 10^3$  cells were inoculated into 96-well plates and transfected with the indicated RNA duplexes. Then, the cells were treated with 10  $\mu$ L of cell counting solution (WST-8, dojindo laboratories, Tokyo) at 0, 24, 48 and 72 h, and then cultured for 2 h. Absorbance values were measured at 450 nm using a microplate reader.

### Luciferase reporter gene assay

Fragments of the cDNAs containing the promoter region of GPX4 were amplified by PCR and were cloned into the Sall and bamHI restriction sites (Promega, USA) of the luciferase report gene of pmir-GLO. PC12 cells were cultured in 24-well culture plates for 12 h and then recombinant plasmids were co-transfected together with RXR $\gamma$  or empty vector into cells. The co-transfected cells were lysed

using the Reporter Lysis Buffer. The luciferase activity of each sample was measured using the Dual-Luciferase Reporter Assay System (Promega, WI, USA).

### Chromatin immunoprecipitation (ChIP) Assay

ChIP was performed using the commercial ChIP kit (Cell signaling technology, USA) according to the manufacturer's protocol. For each chromatin immunoprecipitation, 5  $\mu$ g of anti-FOXC1 and 1  $\mu$ L of normal rabbit IgG were used. IgG antibody was included as a negative control. After immunoprecipitation, chromosomal DNA was purified. Enrichment of ELAVL1 promoter region was detected by using qRT-PCR.

### Iron level detection assay

Intracellular iron level was determined with the standard Iron assay kit (Abcam, USA) according to the manufacturer's protocol. Cultured or transfected cells following treatments were lysed with RIPA lysis buffer supplemented with protease inhibitor. Protein concentration in extracted lysate was quantified with the pierce BCA protein Assay (Thermo Fisher Scientific, USA). Iron levels in the extracted lysate was similarly quantified with the Iron assay kit. Iron level in protein lysate was calculated. The iron level detection method in tissue homogenates was the same as above.

### Cellular glutathione (GSH) and oxidized glutathione (GSSG) detection

Intracellular GSH and GSSG levels were measured with the standard GSH and GSSG detection assay kits (Nanjing Jiancheng Bioengineering Institute, China) according to the manufacturer's instruction. The PC12 cells ( $1 \times 10^5$  /well) were seeded into 24-well plates and cultured overnight. Then, treated cells were collected and broken, supernatants were well mixed with precipitant, buffer and developer. After standing for 5 min, the absorbance at 450 nm was measured using a microplate reader. The levels of GSH in mouse brain tissues were measured following the described protocol above.

### 5-triphenyl-tetrazolium-chloride (TTC) staining

Brains were isolated and cut into 2-mm-thick coronal sections. The sections were incubated in a 2% TTC solution for 30 min at 37 °C in the dark. The staining process was stopped by 4% paraformaldehyde in PBS. The stained sections were scanned after 12 h, and the infarct volume was determined by image analysis and expressed as the percentage of the whole cerebral tissue.

## Morris water maze

In order to study spatial memory and learning, the Morris Water Maze (MWM) was conducted in a quiet environment. At room temperature, a 55 cm high and 160 cm diameter cycloid pool was filled with water to a depth of 23 cm. A circular plexiglass escape platform (10 cm in diameter) was placed in the center of a quadrant of the pool. The experiment consisted of two stages, including five consecutive training days and four measurement days. During the training day, the animals were tested four times, with the platform immersed 1.5 cm below the water surface (the longest test duration was 60 s; the interval was 20–30 min). The delay to the platform was analyzed to evaluate the learning situation of the mice.

## Morphology of mitochondria observed by transmission electron microscope (TEM)

Cells were fixed with 2% osmic acid for 2 h, and then dehydrated with 50%, 70%, 80% and 90% ethanol gradient for 15 min respectively (overnight in 70% ethanol), and then dehydrate with 100% ethanol for 3 times for 20 min each time. After replaced with acetone twice for 15 min each time, the cells were impregnated with following reagents: acetone: impregnation solution with embedding agent = 1:2 for 4 h; the pure embedding agent is impregnated twice for 4 h each time. Then the samples were put into the embedding plate containing pure embedding agent, placed at 65 °C for more than 48 h, and sectioned with a surface area less than 0.2 mm × 0.2 mm. Finally, the sections were stained with 3% uranium acetate lead

citrate double staining, and morphology of mitochondria observed by a FEI Scios 2 DualBeam TEM (Thermo Fisher).

## Statistical analysis

SPSS 21.0 (SPSS, Inc, Chicago, IL) was used for statistical analysis. All the results were expressed as mean ± mean square error (SEM). Three independent experiments were conducted for each experiment. The significance of the differences was analyzed by Student's t-test (two groups) unless special attention was paid to paired comparison or ANOVA (three or more groups) followed by Duncan test.  $P < 0.01$  was considered to be statistically significant.

## Results

### RXR $\gamma$ and GPX4 protein levels were downregulated, COX-2 level was upregulated and cell viability was inhibited in A/R induced PC12 neurons

In order to investigate the expression of RXR $\gamma$  in A/R induced neurons, we detected the RXR $\gamma$  level in PC12 cells. RXR $\gamma$  protein level was downregulated in A/R induced cells, and it was time-dependent (Fig. 1A and B). Iron ion contents were increased in A/R treated cells. In particular, the effect of A/R treatment for 24 h was the most obvious (Fig. 1C). COX-2 protein level was upregulated, and GPX4

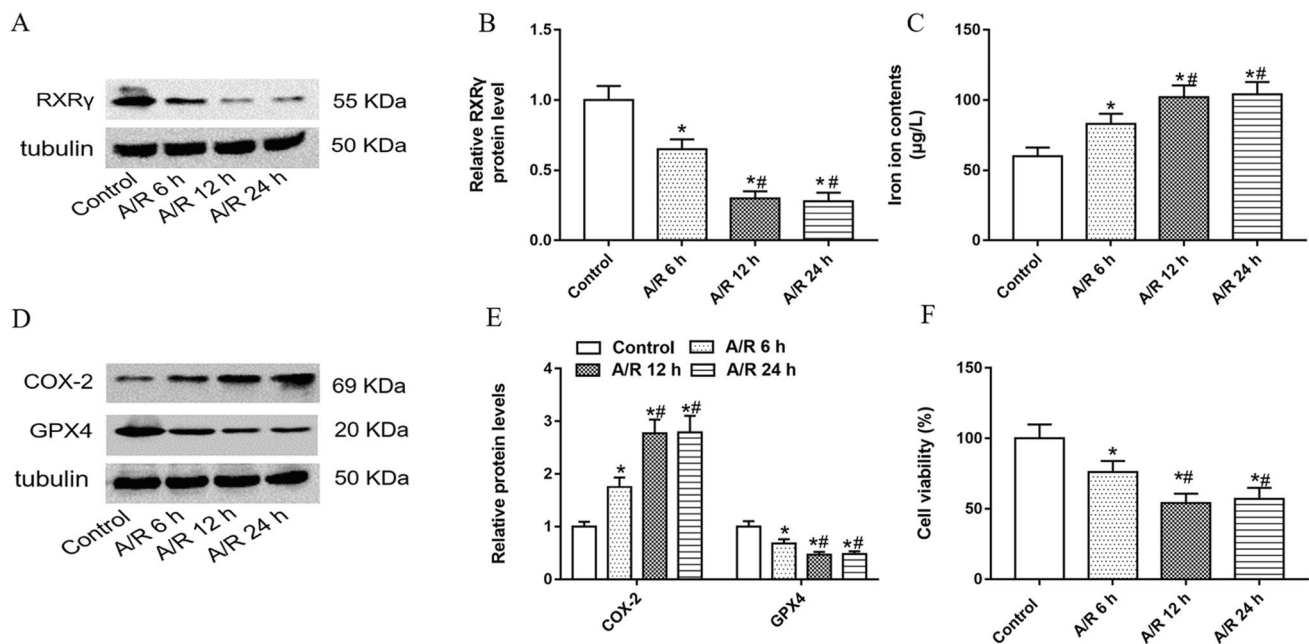


**Fig. 1** Effect of A/R treatment on the expression levels of A/R on RXR $\gamma$ , GPX4 and COX-2 and iron ion contents in PC12 neurons. PC12 cells were treated with A/R for 6, 12 and 24 h: (A and B) RXR $\gamma$  protein level was measured in PC12 cells with Western blot

assay. \* $P < 0.01$  versus control; # $P < 0.01$  versus A/R 6 h. (C) Iron ion contents were detected with a iron assay kit. (D and E) COX-2 and GPX4 protein levels were measured with Western blot assay. (F) Cell viability was detected with CCK-8 assay in cells

level was downregulated in A/R treated cells (Fig. 1D and E). As shown in Fig. 1F, cell viability was downregulated in A/R treated cells, and it was time-dependent. These results suggested that A/R treatment might cause ferroptosis in PC12 cells.

### ROS level was increased in A/R induced neurons

ROS level was increased in A/R treated cells, and it was time-dependent (Fig. 2A and B). Immunofluorescence assay showed that MAP2, a specific neuron cytoskeletal protein, was highly expressed in hippocampal neurons (Fig. 2C). Immunofluorescence assay confirmed that RXR $\gamma$  was located in the nucleus and was downregulated by A/R treatment in a time-dependent manner (Fig. 2D).

### Knockdown of RXR $\gamma$ downregulated RXR $\gamma$ and GPX4 protein level, and upregulated COX-2 level in A/R induced cells

In order to explore the mechanism of ferroptosis, 0.2 or 0.5  $\mu\text{g/mL}$  RXR $\gamma$  shRNA was transfected into normal mouse

hippocampal nerve cells. As shown in Fig. 3A and B, RXR $\gamma$  protein level was downregulated in cells transfected with RXR $\gamma$  shRNA, and 0.2  $\mu\text{g/mL}$  RXR $\gamma$  shRNA was more effective than 0.5  $\mu\text{g/mL}$ . Subsequently, we detected changes in other proteins related to ferroptosis in the cells. RXR $\gamma$  knockdown downregulated GPX4 level and upregulated COX-2 level (Fig. 3C and D). Moreover, RXR $\gamma$  knockdown increased ROS level, and the effect of 0.5  $\mu\text{g/mL}$  was better than that of 0.2  $\mu\text{g/mL}$  (Fig. 3E and F).

### RXR $\gamma$ overexpression upregulated RXR $\gamma$ and GPX4 levels, and downregulated COX-2 level in A/R treated cells

0.5 or 1  $\mu\text{g/mL}$  RXR $\gamma$  was transfected into A/R treated cells. RXR $\gamma$  protein level was decreased in A/R treated cells, and 0.5 or 1  $\mu\text{g/mL}$  RXR $\gamma$  overexpression vector (RXR $\gamma$ ) treatment increased RXR $\gamma$  level (Fig. 4A and B). Moreover, we measured GPX4 and COX-2 protein levels in A/R treated cells, and the results confirmed that RXR $\gamma$  overexpression increased GPX4 protein level and downregulated COX-2 level compared with cells treated with A/R for 24 h, and 1  $\mu\text{g/mL}$  RXR $\gamma$

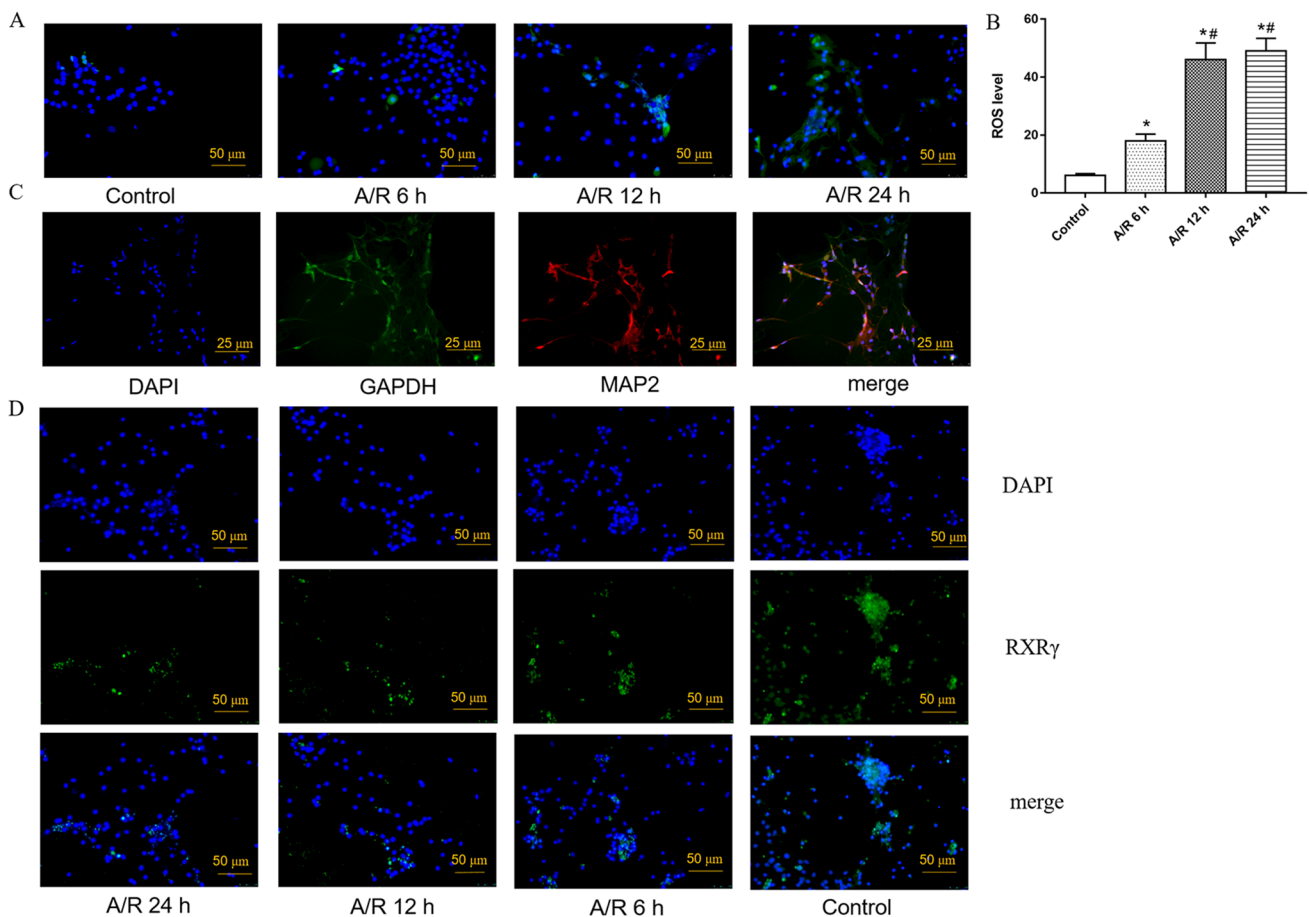


**Fig. 2** ROS level was increased in A/R induced PC12 cells. (A and B) DCFH-DA was used to determine the intracellular ROS levels. \* $P < 0.01$  versus control; # $P < 0.01$  versus A/R 6 h. (C) Immunofluorescence assay used to measure MAP2 expression of neuron dendrite marker at 24 h. (D) RXR $\gamma$  protein localization was determined with immunofluorescence assay

relevance assay used to measure MAP2 expression of neuron dendrite marker at 24 h. (D) RXR $\gamma$  protein localization was determined with immunofluorescence assay

overexpression vector treatment was more effective than 0.5  $\mu\text{g}/\text{mL}$  (Fig. 4C and D). RXR $\gamma$  overexpression decreased ROS level in A/R induced cells, and 1  $\mu\text{g}/\text{mL}$  RXR $\gamma$  overexpression vector was better than 0.5  $\mu\text{g}/\text{mL}$  (Fig. 4E and F).

### RXR $\gamma$ positively regulated GPX4 level

To further explore the mechanism of RXR $\gamma$  regulating A/R, we applied online software (<http://jaspar.genereg.net/>) to predict the relationship between RXR $\gamma$  and GPX4, and found that there are two motifs of RXR $\gamma$  in the GPX4 promoter (-363~-346;-211~-198) (Fig. 5A). In addition, Luciferase report gene and ChIP assays verified that RXR $\gamma$  could bind with GPX4 promoter (Fig. 5B and C). Subsequently, we measured GPX4 mRNA level and found that RXR $\gamma$  overexpression enhanced GPX4 mRNA level and RXR $\gamma$  knockdown inhibited GPX4 mRNA level (Fig. 5D).

### Knockdown of GPX4 reduced the damage to mitochondria caused by overexpression of RXR $\gamma$ and reversed the decrease of iron ion concentration in A/R treated cells

Then, we investigate the involvement of RXR $\gamma$  and GPX4 in the regulation of A/R-induced ferroptosis. Since the main characteristics of ferroptosis in the subcellular morphology changes are significant reduction in mitochondria size, increase in mitochondrial membrane density and decrease in cristae. We transfected RXR $\gamma$  overexpression vector and GPX4 shRNA into A/R-treated PC12 cells individually or jointly, and TEM was applied to observe the mitochondria morphology. The results showed that RXR $\gamma$  overexpression obviously improve the mitochondria morphology, while GPX4 aggravated mitochondrial atrophy and could reverse the improvement of morphology by RXR $\gamma$  overexpression

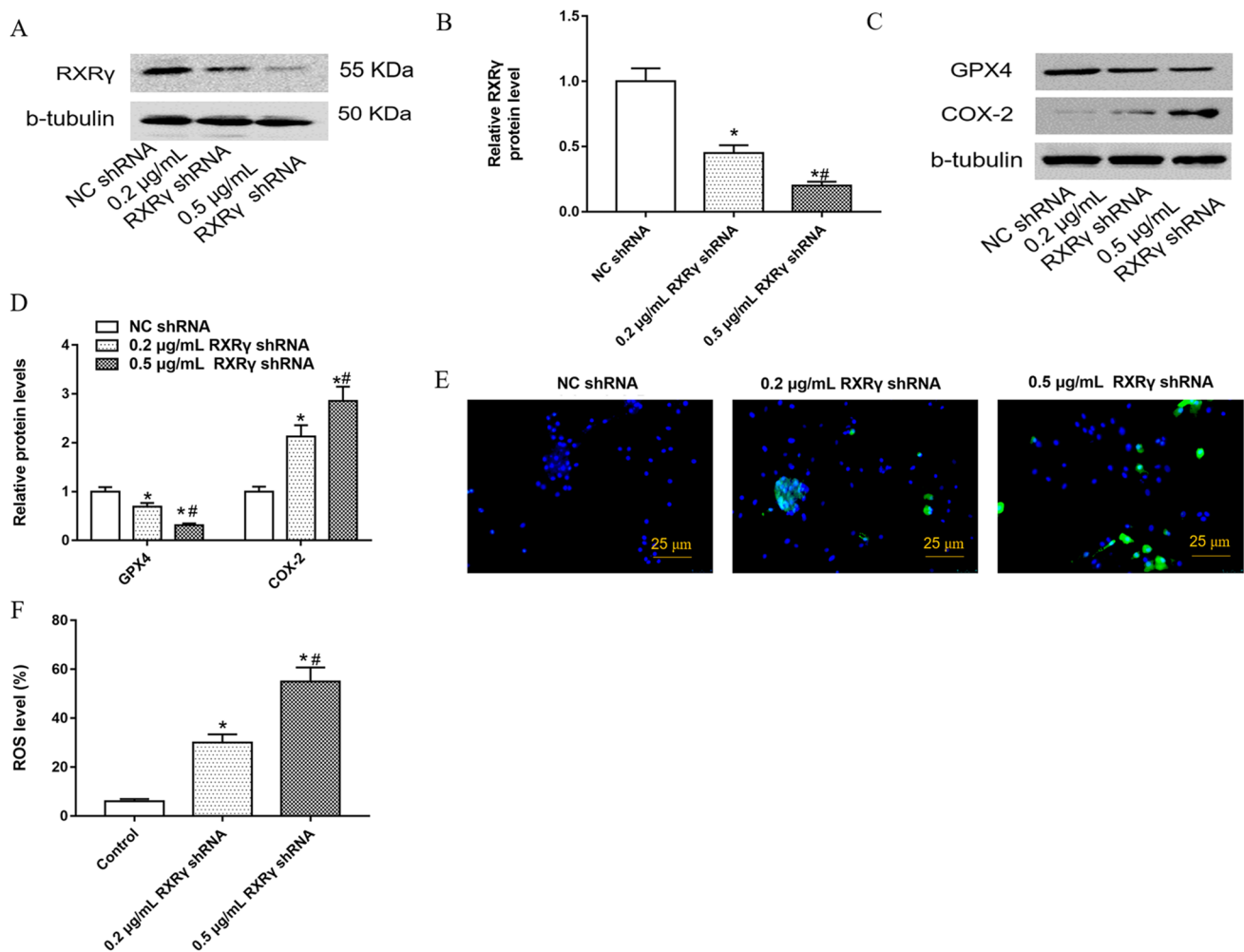


**Fig. 3** Effect of RXR $\gamma$  knockdown on RXR $\gamma$ , GPX4 and COX-2 protein levels. 0.2 or 0.5  $\mu\text{g}/\text{mL}$  RXR $\gamma$  shRNA and the negative control (NC shRNA) were transfected into A/R treated PC12 cells: RXR $\gamma$  (A and B), GPX4 and COX-2 (C and D) protein levels were measured with Western blotting.

(E) DCFH-DA was used to determine the intracellular ROS levels. \* $P < 0.01$  versus control; \*\* $P < 0.01$  versus 0.2  $\mu\text{g}/\text{mL}$  RXR $\gamma$  shRNA

(Fig. 6A). GPX4 knockdown reversed the upregulation of RXR $\gamma$  overexpression on the upregulation of GPX4 expression and downregulation of COX-2 level in A/R treated cells (Fig. 6B and C). RXR $\gamma$  overexpression increased ROS level compared with cells treated with Vector, and GPX4 knockdown reversed the increase of RXR $\gamma$  overexpression on ROS level in A/R treated cells (Fig. 6D). Moreover, we found that RXR $\gamma$  overexpression decreased iron ion concentration, and GPX4 knockdown increased iron ion concentration (Fig. 6E).

### Knockdown of GPX4 reverses the protective effect of overexpression of RXR $\gamma$ on neurological function in I/R mice

We then verified the role of RXR $\gamma$  in vivo. Water maze results demonstrated that escape latency was extended in I/R mice. Administration with LV-RXR $\gamma$  shortened the escape latency, and knockdown of GPX4 extended the escape latency (Fig. 7A and B). Cerebral infarct size and degree of brain damage were increased in I/R mice, and overexpression of RXR $\gamma$  or GPX4

decreased the cerebral infarct size and brain damage degree (Fig. 7C and D).

### Knockdown of GPX4 reversed the inhibitory effect of overexpression of RXR $\gamma$ on oxidative stress and iron ion concentration in brain tissue of I/R mice

ROS level was enhanced in I/R mice. Administration with LV-RXR $\gamma$  or LV-GPX4 decreased ROS level (Fig. 8A). Western blot assay detected that COX-2 level was upregulated in I/R mice, and overexpression of RXR $\gamma$  and GPX4 could both suppress I/R-induced COX-2 expression (Fig. 8B). GPX4 level was downregulated in I/R mice, and overexpression of RXR $\gamma$  and GPX4 could both improve I/R-induced suppression of GPX4 expression (Fig. 8B). Iron ion contents were increased in I/R rats compared with mice in sham group, and overexpression of RXR $\gamma$  and GPX4 could both improve I/R-induced Iron ion contents (Fig. 8C). GSH level/GSSG level and SOD activity were decreased in I/R mice, and overexpression of RXR $\gamma$  and GPX4 could both

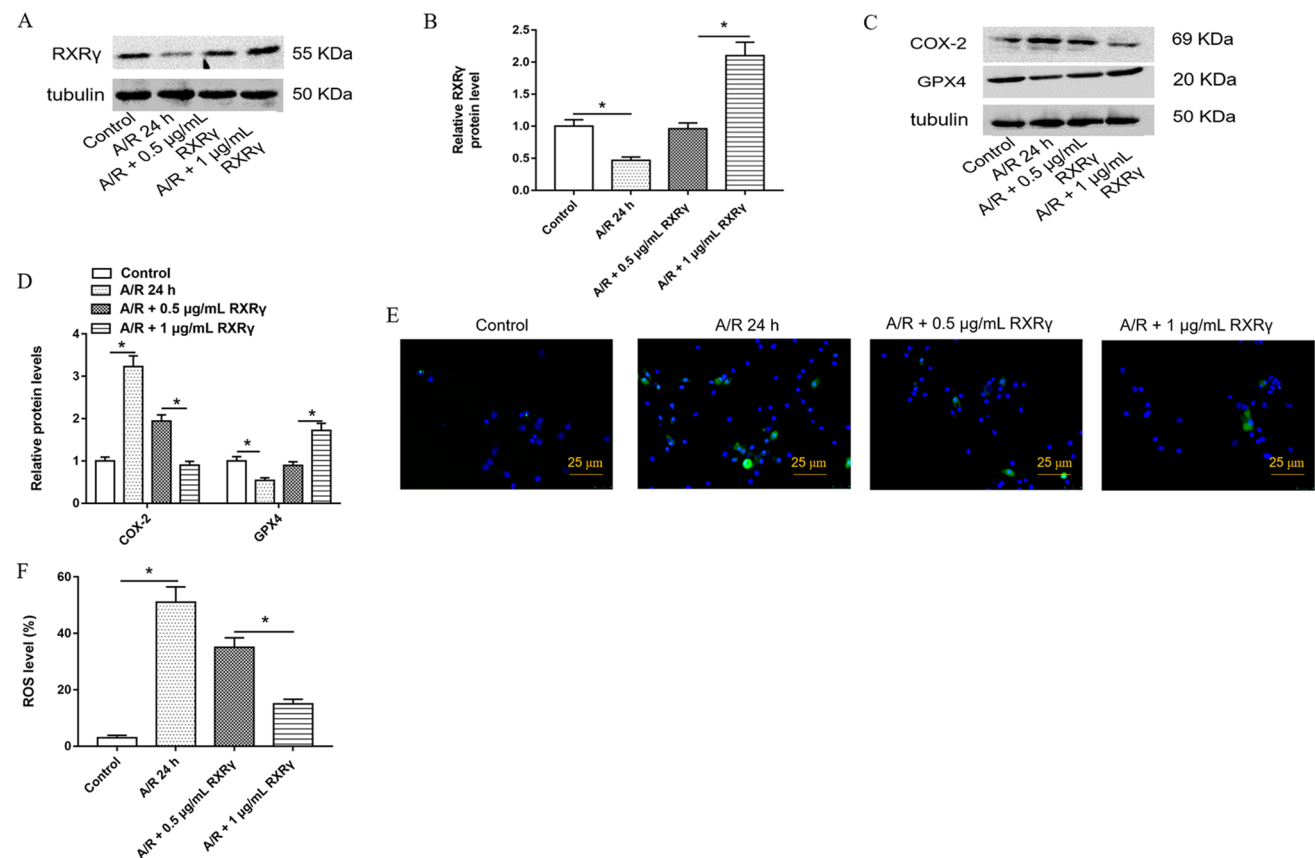


**Fig. 4** Effect of RXR $\gamma$  overexpression on RXR $\gamma$ , COX-2 and GPX4 protein levels in A/R treated cells. PC12 cells were transfected with 0.5 or 1  $\mu$ g/mL pcDNA-RXR $\gamma$  overexpression vector, and after 24 h, the cells were treated with A/R for another 24 h: RXR $\gamma$  (A

and B), GPX4 and COX-2 (C and D) protein level was measured in PC12 cells with Western blot assay. (E and F) DCFH-DA was used to determine the intracellular ROS levels. \* $P$ <0.01 versus control group or A/R + 0.5  $\mu$ g/mL RXR $\gamma$  group



improve I/R-induced suppression of GSH level/GSSG level and SOD activity (Fig. 8D and E).

## Discussion

Cerebrovascular diseases such as atherosclerosis are diseases with the highest mortality throughout the world (Shao et al. 2016). At present, the treatment of cerebral ischemia is limited, and its damage is usually irreversible. Here, we studied ferroptosis and RXR $\gamma$  role in brain I/R. We confirmed that ferroptosis was induced and RXR $\gamma$  level was downregulated during cerebral I/R. RXR $\gamma$  overexpression inhibited ferroptosis and cerebral I/R injury. RXR $\gamma$  bound to the GPX4 promoter region and activated the transcription of GPX4 during cerebral I/R.

I/R causes a decrease in the arterial blood supply to the tissues, followed by restoration of perfusion and subsequent

re-oxygenation. The reconstitution of blood flow causes further damage to ischemic tissues through the accumulation of ROS, interference with cell ion homeostasis, and inflammatory response to cell death (Liew et al. 2015; Wang et al. 2021a). Under normal circumstances, ROS mediated important beneficial reactions. When their production was prolonged or increased, harmful events with special cellular changes were observed. Studies have shown that during I/R, ROS can stimulate tissue inflammation and induce the activation of NLRP3 inflammasomes (Abais et al. 2015; Qiu et al. 2017). In this process, NLRP3 may directly sense the presence of ROS produced indirectly by normal or malfunctioning mitochondria or other activators of NLRP3 (Yu and Lee 2016). Our results revealed that PC12 cells induced with A/R increased ROS level, and GPX4 knockdown reversed the effect of overexpression of RXR $\gamma$  on the suppression of ROS levels in PC12 cells induced by A/R.

Ferroptosis is an iron-dependent cell death (Yang and Stockwell 2016), which reduces the antioxidant capacity, leads to the

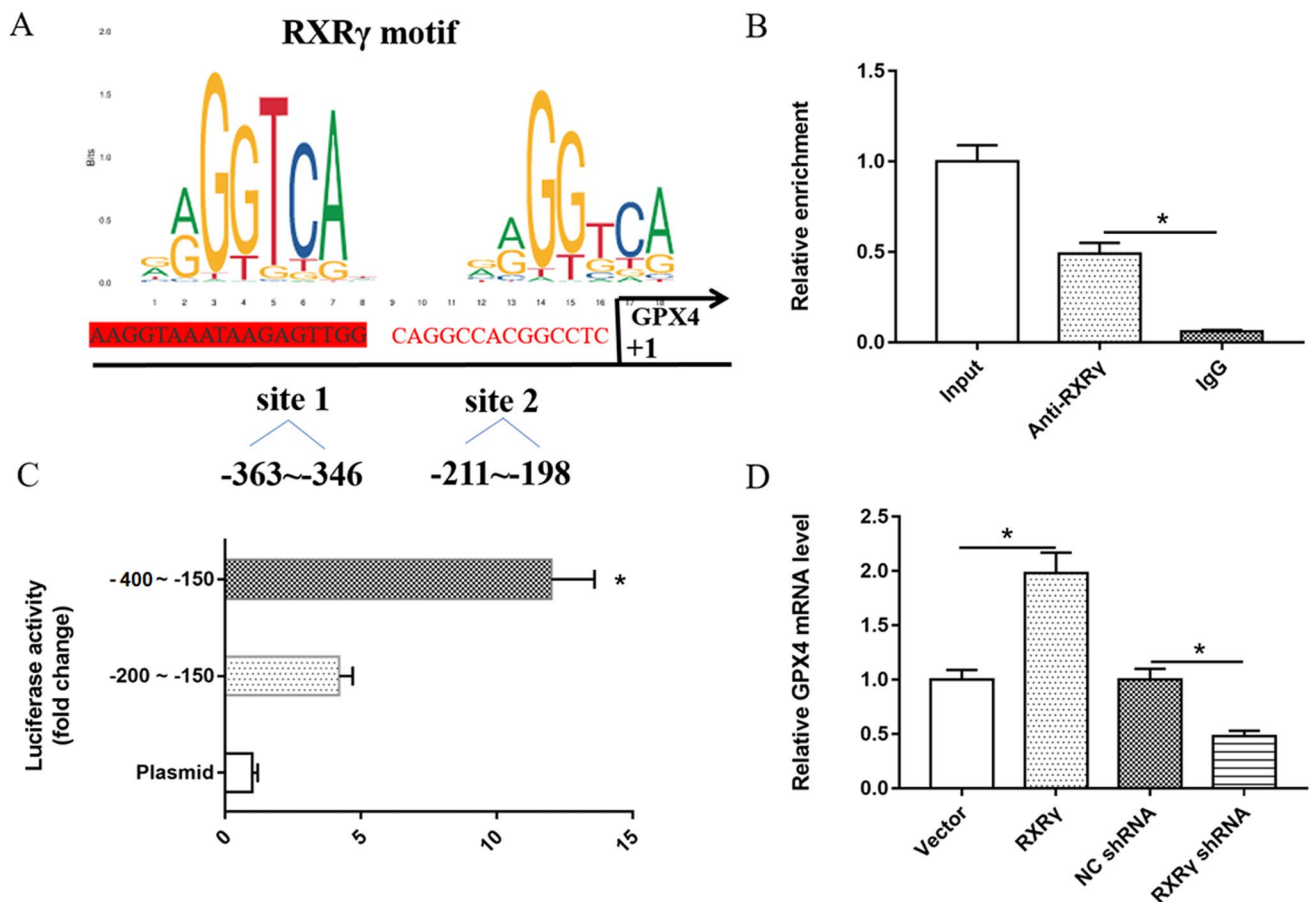


**Fig. 5** The relationship between RXR $\gamma$  and GPX4. (A) Online system (<http://jaspar.genereg.net/>) was used to predict the relationship between RXR $\gamma$  and GPX4 promoter. (B) ChIP assay was used to measure the binding ability of RXR $\gamma$  and GPX4 promoter. \* $P < 0.01$  versus anti-RXR $\gamma$  group. (C) Luciferase reporter gene assay was used

to verify the relationship between RXR $\gamma$  and GPX4. \* $P < 0.01$  versus -200~-150 bp group. PC12 cells induced with A/R were treated with pcDNA-RXR $\gamma$  (RXR $\gamma$ ), RXR $\gamma$  shRNA and their negative controls (Vector and NC shRNA): (D) GPX4 mRNA level was detected with RT-qPCR. \* $P < 0.01$  versus vector or NC shRNA

accumulation of lipid ROS, and ultimately leads to the death of oxidized cells. Ferroptosis is related to neurodegenerative diseases (Alzheimer's disease and Parkinson's disease), cancer and kidney degeneration. Most enzymes and proteins that cascade or interact in the ferroptosis pathway, such as the cystine/glutamate transporter xc-, GPX4 and glutamate half Cystine ligase (GCLC) iron metabolism gene transferrin receptor 1 (TFR1) subunit of iron transporter, heme oxygenase 1 (HO-1) and ferritin are protected by the transcription factor Nrf2 oxidation reaction element adjustment (Kajarabille and Latunde-Dada 2019; Seibt et al. 2019; Fang et al. 2020; Tang et al. 2021). The researches of ferroptosis in I/R injury are not so extensive, and the specific function remains to be studied. Here, we provided strong evidence that cerebral I/R surgery induced nerve cell ferroptosis. We observed increased cellular iron level and ROS level after brain I/R injury or A/R exposure, accompanied by the downregulation of GPX4 level and upregulation of COX-2

level. In addition, we found that ferroptosis plays an important role in cerebral I/R injury. Inhibition of ferroptosis could significantly reduce damage. Therefore, ferroptosis can be used as a protective target for cerebral I/R injury.

It was reported that the RXR agonist bexarotene improved the level of Ym1 immunopositive N2 neutrophils in the ipsilateral cerebral hemisphere and spleen of mice with transient middle cerebral artery occlusion, and confirmed that bexarotene played a peripheral immunomodulatory role under ischemic conditions and could be effectively used in the acute treatment of ischemic stroke (Certo et al. 2015). According to one report, RXR activation can effectively protect lung tissue from I/R damage, and its mechanism may be associated with activation of the Nrf2 signaling pathway, enhancement of antioxidant levels, and reduction of oxidative stress (Xiang et al. 2019). Our results confirmed that RXR $\gamma$  attenuated cerebral I/R by

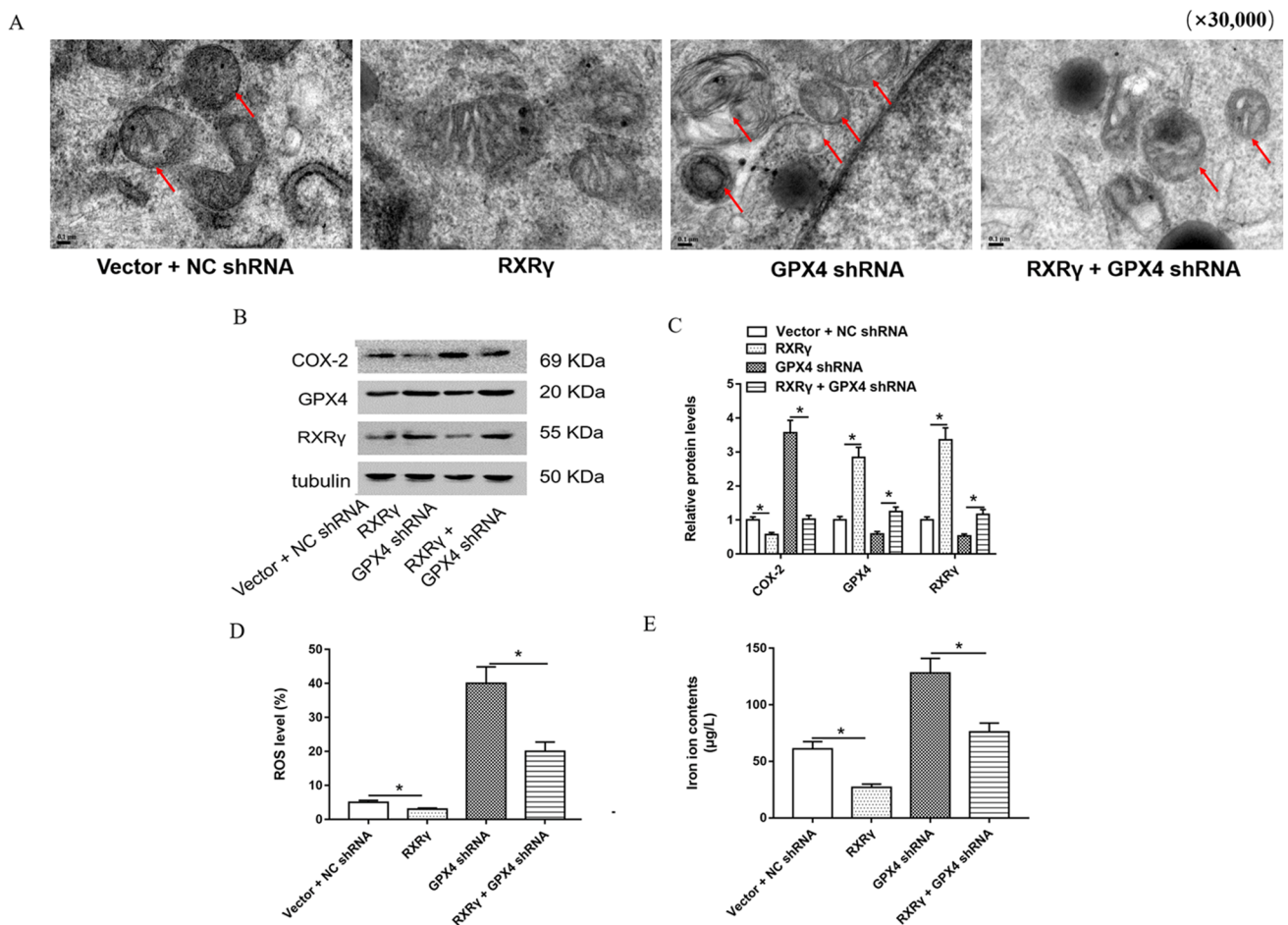


**Fig. 6** Effect of GPX4 knockdown on the influence of mitochondria morphology, ROS production, Cox-2, GPX4 and RXR $\gamma$  protein levels in A/R-treated PC12 cells. PC12 cells induced with A/R were treated with 1  $\mu$ g/mL pcDNA-RXR $\gamma$  (RXR $\gamma$ ) alone or together with 0.5  $\mu$ g/mL GPX4 shRNA: (A) The ultrastructure of mitochondria was observed. (B and C) COX-2, GPX4 and RXR $\gamma$  protein levels were

measured in cells. \* $P$  < 0.01 versus vector or RXR $\gamma$  + NC shRNA. (D) DCFH-DA was used to determine the intracellular ROS levels. \* $P$  < 0.01 versus vector or RXR $\gamma$  + NC shRNA. (E) Iron ion contents were detected with an iron assay kit in cells. \* $P$  < 0.01 versus vector or RXR $\gamma$  + NC shRNA

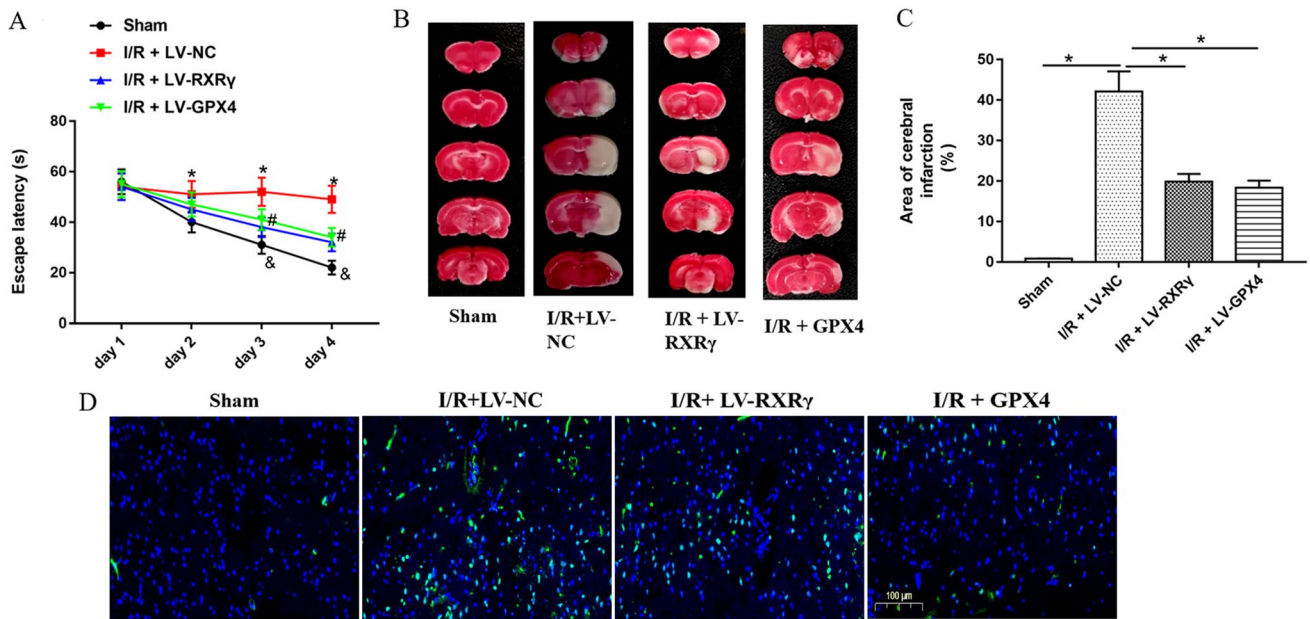


**Fig. 7** Effect of GPX4 overexpression or RXR $\gamma$  overexpression on brain injury in I/R mice. I/R mice were administrated with LV-RXR $\gamma$ , LV-GPX4 or LV-NC: **(A)** The learning and memory ability of mice were detected with Morris water maze. **(B)** Escape latency was meas-

ured in mice. **(C)** TTC staining was used to detect area of cerebral infarction of mice. **(D)** TUNEL staining was used to measure apoptotic cell proportion in brain tissues. \* $P < 0.01$

transcriptionally promoting the expression of GPX4, including reducing the level of ROS in cells, reducing the content of the Fe ion, and downregulation of COX-2 level. Here,

we identified GPX4 as a new target gene of RXR $\gamma$ . RXR $\gamma$  directly bound to the GPX4 promoter region and promoted GPX4 transcription.

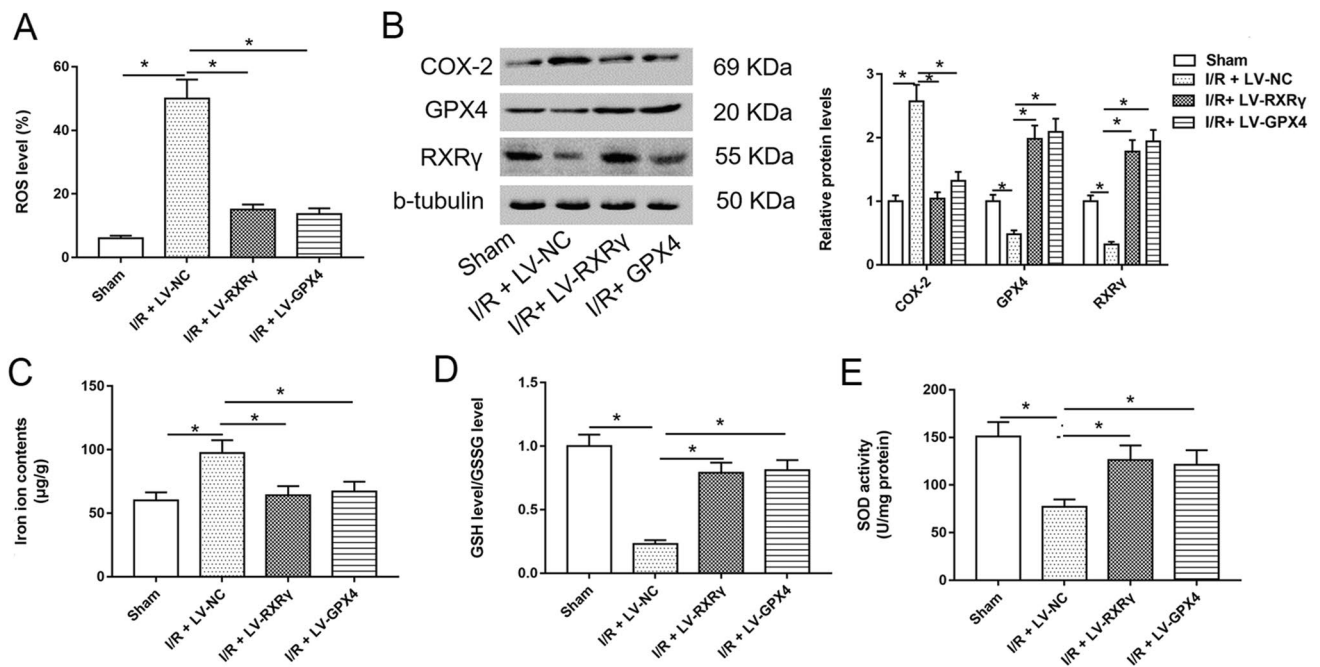


**Fig. 8** Effects of GPX4 overexpression or RXR $\gamma$  overexpression on oxidative stress and iron ion contents in I/R mice. **(A)** DCFH-DA was used to determine the ROS levels in the brain tissue. **(B)** COX-2, GPX4 and RXR $\gamma$  protein levels were measured in the brain with

Western blot assay. **(C)** Iron ion contents were detected with an iron assay kit in mouse brain. **(D)** and **(E)** ELISA kits were used to detect GSH/GSSG level and SOD activity in mouse brain. \* $P < 0.01$

There are some limitations in our study. Firstly, in vitro cultures do not have comorbidities which are the major concern when treating comorbid patients, since ischemia–reperfusion injury is of so complex pathological mechanism that all the factors cannot be applied to cells in vitro and even we do not know clearly all the factors (Popa-Wagner et al. 2020). Secondly, the mechanism verified in the in vitro studies may not translate the in vivo situations very well, due to the complexity and compensation of the body's microenvironment (Popa-Wagner et al. 2020; Wang et al. 2020). Moreover, specific indexes of tissue ferroptosis are now inconclusive (Hirschhorn and Stockwell 2019; Sun et al. 2020), so it is also difficult for us to apply the in vitro mechanism to the in vivo situations. Finally, some scholars believe that aged rodent model is closer to human stroke, because aging is a very important and common risk factor for stroke (Joseph et al. 2012; Penlioglou et al. 2021). Of course, we agree with them, but we used young mice in this study and believe it is not absolutely inappropriate. Because, aging is not the unique risk factor for stroke, and many researchers also used young mice or rats in their studies.

## Conclusions

RXR $\gamma$  attenuates cerebral ischemia–reperfusion induced ferroptosis in neurons in mice through transcriptionally promoting the expression of GPX4.

**Author contribution** LY performed experiments, collected data and drafted the manuscript. BD analyzed the data. SZ contributed the methodology. MW conceived and designed research. All authors read and approved the final manuscript.

**Data availability statement** The datasets used and analyzed during the current study are available from the corresponding author on reasonable request.

## Declarations

**Conflict of interest** The authors declare that there is no conflict of interest regarding the publication of this paper.

## References

- Abais JM, Xia M, Zhang Y, Boini KM, Li PL (2015) Redox regulation of NLRP3 inflammasomes: ROS as trigger or effector? *Antioxid Redox Signal* 22(13):1111–1129
- Bi J, Zhang J, Ren Y, Du Z, Li Q, Wang Y et al (2019) Irisin alleviates liver ischemia-reperfusion injury by inhibiting excessive mitochondrial fission, promoting mitochondrial biogenesis and decreasing oxidative stress. *Redox Biol* 20:296–306
- Burton MD, Sparkman NL, Johnson RW (2011) Inhibition of interleukin-6 trans-signaling in the brain facilitates recovery from lipopolysaccharide-induced sickness behavior. *J Neuroinflammation* 8:54
- Certo M, Endo Y, Ohta K, Sakurada S, Bagetta G, Amantea D (2015) Activation of RXR/PPAR $\gamma$  underlies neuroprotection by bexarotene in ischemic stroke. *Pharmacol Res* 102:298–307
- Dai S, Hua Y, Keep RF, Novakovic N, Fei Z, Xi G (2019) Minocycline attenuates brain injury and iron overload after intracerebral hemorrhage in aged female rats. *Neurobiol Dis* 126:76–84
- Ding C, Ding X, Zheng J, Wang B, Li Y, Xiang H et al (2020) miR-182-5p and miR-378a-3p regulate ferroptosis in I/R-induced renal injury. *Cell Death Dis* 11(10):929
- Duan J, Cui J, Zheng H, Xi M, Guo C, Weng Y et al (2019) Aralia taibaiensis Protects against I/R-Induced Brain Cell Injury through the Akt/SIRT1/FOXO3a Pathway. *Oxid Med Cell Longev* 2019:7609765
- Fang X, Cai Z, Wang H, Han D, Cheng Q, Zhang P et al (2020) Loss of Cardiac Ferritin H Facilitates Cardiomyopathy via Slc7a11-Mediated Ferroptosis. *Circ Res* 127(4):486–501
- Forcina GC, Dixon SJ (2019) GPX4 at the Crossroads of Lipid Homeostasis and Ferroptosis. *Proteomics* 19(18):e1800311
- Girardi CS, Rostrolla DC, Lini FJM, Brum PO, Delgado J, Ribeiro CT et al (2019) Nuclear RXR $\alpha$  and RXR $\beta$  receptors exert distinct and opposite effects on RA-mediated neuroblastoma differentiation. *Biochim Biophys Acta Mol Cell Res* 1866(3):317–328
- Hirschhorn T, Stockwell BR (2019) The development of the concept of ferroptosis. *Free Radic Biol Med* 133:130–143
- Joseph C, Buga AM, Vintilescu R, Balseanu AT, Moldovan M, Junker H, Walker L, Lotze M, Popa-Wagner A (2012) Prolonged gaseous hypothermia prevents the upregulation of phagocytosis-specific protein annexin 1 and causes low-amplitude EEG activity in the aged rat brain after cerebral ischemia. *J Cereb Blood Flow Metab* 32(8):1632–1642
- Kajarabille N, Latunde-Dada GO (2019) Programmed Cell-Death by Ferroptosis: Antioxidants as Mitigators. *Int J Mol Sci* 20(19):4968
- Kalogeris T, Baines CP, Krenz M, Korthuis RJ (2016) Ischemia/reperfusion. *Compr Physiol* 7(1):113–170
- Li S, Qian ZM, Xu G, Zheng J, Wu Y (2020) Hepatocyte growth factor protects PC12 cells against OGD/R-induced injury by reducing iron. *Biosci Rep* 40(4):BSR20200287
- Liew HK, Kuo JS, Wang JY, Pang CY (2015) Granulocyte-Colony Stimulating Factor Increases Cerebral Blood Flow via a NO Surge Mediated by Akt/eNOS Pathway to Reduce Ischemic Injury. *ScientificWorldJournal* 2015:657932
- Lu J, Xu F, Lu H (2020) LncRNA PVT1 regulates ferroptosis through miR-214-mediated TFR1 and p53. *Life Sci* 260:118305
- Maiorino M, Conrad M, Ursini F (2018) GPX4, Lipid Peroxidation, and Cell Death: Discoveries, Rediscoveries, and Open Issues. *Antioxid Redox Signal* 29(1):61–74
- Penlioglou T, Stoian AP, Papanas N (2021) Diabetes, Vascular Aging and Stroke: Old Dogs, New Tricks? *J Clin Med* 10(19)
- Popa-Wagner A, Dumitrascu DI, Capitanescu B, Petcu EB, Surugiu R, Fang WH, Dumbrava DA (2020) Dietary habits, lifestyle factors and neurodegenerative diseases. *Neural Regen Res* 15(3):394–400
- Qiu Z, Lei S, Zhao B, Wu Y, Su W, Liu M et al (2017) NLRP3 Inflammasome Activation-Mediated Pyroptosis Aggravates Myocardial Ischemia/Reperfusion Injury in Diabetic Rats. *Oxid Med Cell Longev* 2017:9743280
- Rousselle E, Kriz J, Seidah NG (2012) Mouse model of intraluminal MCAO: cerebral infarct evaluation by cresyl violet staining. *J vis Exp* 69:4038
- Seibt TM, Proneth B, Conrad M (2019) Role of GPX4 in ferroptosis and its pharmacological implication. *Free Radic Biol Med* 133:144–152
- Shao BZ, Han BZ, Zeng YX, Su DF, Liu C (2016) The roles of macrophage autophagy in atherosclerosis. *Acta Pharmacol Sin* 37(2):150–156

- Sun Y, Chen P, Zhai B, Zhang M, Xiang Y, Fang J, Xu S, Gao Y, Chen X, Sui X et al (2020) The emerging role of ferroptosis in inflammation. *Biomed Pharmacother* 127:110108
- Tang LJ, Zhou YJ, Xiong XM, Li NS, Zhang JJ, Luo XJ et al (2021) Ubiquitin-specific protease 7 promotes ferroptosis via activation of the p53/TfR1 pathway in the rat hearts after ischemia/reperfusion. *Free Radic Biol Med* 162:339–352
- Wang C, Börger V, Sardari M, Murke F, Skuljec J, Pul R, Hagemann N, Dzyubenko E, Dittrich R, Gregorius J et al (2020) Mesenchymal stromal cell-derived small extracellular vesicles induce ischemic neuroprotection by Modulating Leukocytes and specifically neutrophils. *Stroke* 51(6):1825–1834
- Wang L, Zhu T, Xu HB, Pu XP, Zhao X, Tian F et al (2021a) Effects of notoginseng leaf triterpenes on small molecule metabolism after cerebral ischemia/reperfusion injury assessed using MALDI-MS imaging. *Ann Transl Med* 9(3):246
- Wang P, Cui Y, Ren Q, Yan B, Zhao Y, Yu P et al (2021b) Mitochondrial ferritin attenuates cerebral ischaemia/reperfusion injury by inhibiting ferroptosis. *Cell Death Dis* 12(5):447
- Xiang BQ, Yan WX, Lou GQ, Gao H, Zhou ZL, Wu YM et al (2019) The regulation of retinoid X receptor-mediated oxidative stress pathway in rat pulmonary ischemia/reperfusion injury. *Sheng Li Xue Bao* 71(2):301–310
- Yang WS, Stockwell BR (2016) Ferroptosis: Death by lipid peroxidation. *Trends Cell Biol* 26(3):165–176
- Yu JW, Lee MS (2016) Mitochondria and the NLRP3 inflammasome: physiological and pathological relevance. *Arch Pharm Res* 39(11):1503–1518

**Publisher's note** Springer Nature remains neutral with regard to jurisdictional claims in published maps and institutional affiliations.